# Measurement of the neutron reflectivity for Bragg reflections off a perfect silicon crystal

T. Dombeck
*Fermilab, Batavia, Illinois 60510*

R. Ringo
*Argonne National Laboratory, Argonne, Illinois 60439*

D. D. Koetke
*Valparaiso University, Valparaiso, Indiana 46383*

H. Kaiser, K. Schoen, and S. A. Werner
*University of Missouri, Columbia, Missouri 65211*

D. Dombeck
*Cornell University, Ithaca, New York 14850*

(Received 31 May 2001; published 5 October 2001)

We have carried out a neutron reflectivity measurement of silicon as a prelude to a search for the neutron electric dipole moment (EDM). Our technique uses multiple Bragg reflections for neutrons near 1.92 Å as they travel down slots cut along the (440) planes of a perfect silicon crystal. For neutrons within the Darwin peak width, a previous measurement places a lower limit on the reflectivity of $R>0.9978$. Our measurement has been performed at the University of Missouri Research Reactor and has resulted in a value of $R=0.999\,976 \pm 0.000\,075$, which yields a value of $R>0.9999$ at the 90% confidence level. This is in agreement with the calculated reflectivity of $R=0.999\,952$ and indicates that as many as 21 000 multiple Bragg reflections are possible before there is a significant loss of neutron intensity. By coupling the EDM to the atomic electric fields on each reflection, we estimate this technique will allow a measurement of the EDM with a sensitivity on the order of $10^{-27}\,e$ cm.

DOI: 10.1103/PhysRevA.64.053607 PACS number(s): 03.75.Be, 03.75.Dg

## I. INTRODUCTION

If discovered, the neutron electric dipole moment (EDM) would be an example of a particle property that violates parity and time symmetry [1]. The most sensitive experimental searches to date have attempted to couple the EDM to an externally applied electric field [2]. Another method pioneered by Shull and Nathans [3] attempted to couple the EDM with atomic electric fields during Bragg scattering. They utilized a single Bragg scatter off a cadmium sulfide crystal but achieved an upper limit on the EDM that was not as sensitive as the external field methods. Recent calculations involving a modified Shull and Nathans technique [4–6] show that the EDM sensitivity may be greatly improved if multiple coherent Bragg reflections can be used. In this paper, we describe an experiment that uses slots cut into a perfect crystal of silicon to show that the neutron reflectivity is sufficiently large to allow tens of thousands of successive Bragg reflections that could ultimately enhance the EDM sensitivity.

One other measurement of the reflectivity ($R$) in silicon was attempted by Schuster, Carlile, and Rauch [7] and Jericha, Carlile, and Rauch [8] in a device utilizing multiple Bragg reflections to store pulses of neutrons. That experiment used the reflections of 6.27 Å neutrons off the (111) planes. However, there were significant neutron losses associated with a glass guide tube surrounding the device and the experiment measured a lower limit of $R>0.9978$ that was substantially less than their calculated value of 0.999 972.

We have performed our measurement of the neutron reflectivity using the interferometer setup on Beam Port B at the 10 MW University of Missouri Research Reactor. We used multiple Bragg scatters of approximately 1.92 Å neutrons down slots cut along the (440) planes in a perfect silicon crystal. Taking advantage of the wide range of wavelengths available in the beam [9], we have achieved multiple reflections numbering from hundreds to thousands by rotating the crystal in the incident beam. Keeping the flight paths constant to reduce systematic backgrounds, we have performed the reflectivity measurement by comparing the neutron survival fraction for long and short slots under the same experimental conditions. As the short slots have one fourth the number of reflections of the long slots, the comparison allows us to place a lower limit on the reflectivity of $R>0.9999$ at the 90% confidence level (c. 1.). This result represents a considerable improvement over the previous lower limit. It also agrees with our calculation of the average reflectivity of 0.999 952 that indicates 21 000 reflections are possible off the (440) planes in Si before a reduction in the neutron count rate by a factor of $1/e$.

We have compared the reflectivity measurement with that made before etching the crystal and have shown that etching greatly improves the reflectivity. This demonstrates the need to properly prepare the crystal to achieve a large number of reflections.

 

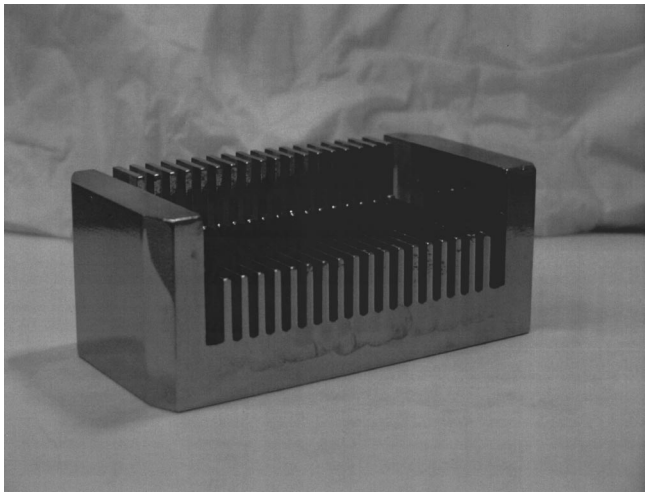

FIG. 1. The photo shows the slotted crystal used for the reflectivity measurement that was fabricated out of a single perfect crystal of silicon. The slots were saw cut into the crystal along the (440) planes.

## II. DESCRIPTION OF THE EXPERIMENT

### A. Apparatus

The central component of the experiment is the slotted crystal shown in Fig. 1. It was fashioned out of a perfect single Si crystal with dimensions: 50 mm wide (along the slot direction), 38 mm high, and 94 mm long. Nineteen slots were saw cut into the crystal along the (440) planes, each 50 mm long and 25.4 mm deep. The 17 central slots have an average width of 2.1 mm while the two end slots have an average width of 4.1 mm to allow clearance for a milling tool. The walls separating the slots have an average thickness of 1.7 mm. The picture in Fig. 1 was taken from the side where the neutrons exit the slots. It can be seen that the upper 12.7 mm of the slots was milled off the top of the walls along the last 37.5 mm. This effectively created two sets of slots: a lower set 12.7 mm deep and 50 mm long, and an upper set 12.7 mm deep and 12.5 mm long, or one fourth the length of the lower set of slots. The slot walls remained joined at their bottoms by a 12.7 mm thick base. Since the entire assembly was fabricated out of a single perfect Si crystal, the crystal planes in the opposing walls of the slots are in register on the angstrom scale. Finally, the exit face of the crystal was cut with a 2° bevel to help ensure that the majority of neutrons exiting the slots would be directed toward the detector. This reduced the average length of the long slots to 48.9 mm and that of the short slots to 12.4 mm.

A schematic diagram of the experimental layout is shown in Fig. 2. The crystal was mounted on a precision rotation table within a vibration isolated box used for neutron interferometry experiments [9]. The orientation of the crystal was such that the incident beam struck the slot entrances at a glancing angle determined by rotating the crystal. Neutrons at the correct wavelength were multiply Bragg scattered down the slots alternately reflecting off the opposing walls. For smaller crystal rotation angles relative to the incident beam, more reflections occurred down the slots, e.g., for a rotation angle near 4° ($\theta_B = 86°$) the neutrons underwent 325

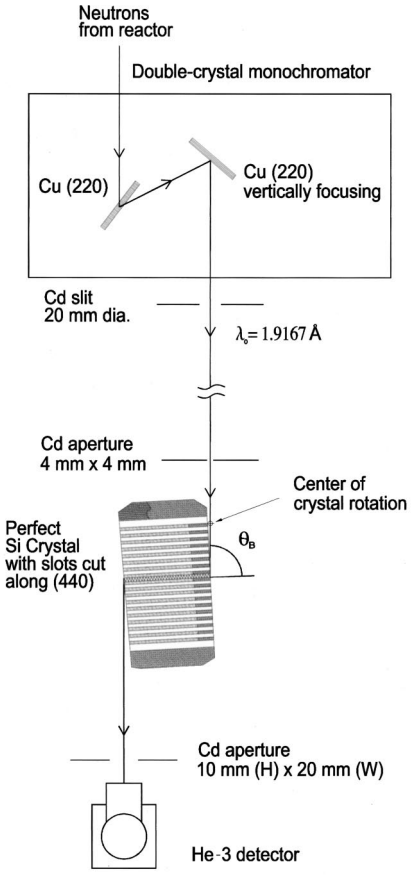


FIG. 2. Schematic diagram of the experimental layout is shown. The reflectivity of the short slots may be measured by lowering the crystal, which leads to a different number of Bragg reflections from the long slots (see Fig. 1 and description in the text).

Bragg reflections down the 50 mm long slots and this increased to 1300 reflections for 1° ($\theta_B = 89°$).

A general description of the beam in Beam Port B is given in Ref. [9]. The beam is confined to neutrons with wavelengths less than 2 Å and we designed our experiment to use wavelengths near 1.92 Å to match the normal reflection off the (440) planes in Si. A double-crystal Cu monochromator system prepared an incident beam with a wavelength spread $\Delta\lambda/\lambda_0 \cong 1\%$ full width at half maximum and an incident intensity of $\Phi \approx 2.9 \times 10^5$ n/cm$^2$/s at 1.92 Å.

The incident beam was restricted by a 4 mm by 4 mm Cd aperture placed just in front of the crystal. The horizontal and vertical beam divergences were measured using a standard technique of passing a narrow slit through the beam at different distances from the Cd aperture and measuring the resulting count rates at each slit position. From the resulting profile widths we calculated that the horizontal beam divergence was $\Delta\Theta_H = 11$ mrad and the vertical beam divergence was $\Delta\Theta_V = 6$ mrad.

The incident beam elevation was centered on the lower set of 50 mm long slots. The crystal could be lowered by 12.7 mm on the rotation table to center the neutron beam on the shorter length slots. On the exit side of the crystal, the neutrons from the slots were directed toward a 25.4 mm diameter $He^3$ detector encased in neutron absorbing material

($B_4C$ epoxy) except for a 10 mm ($H$) by 20 mm ($W$) aperture whose vertical position was centered on the incident neutron beam. The perpendicular distance from the Cd aperture to the detector was 136 mm and during the reflectivity measurement, the detector was translated a distance of 50 mm out of the incident beam to intercept the neutrons that reflected down the crystal slots.

As can be seen from Fig. 1, when the neutrons excited the shorter slots they reflected between two end slabs that contained the neutrons and reflected them toward the stationary detector. Even though the total number of reflections at a given Bragg angle was less for the short slots than for the long slots, the flight path between the two end slabs ensured that the total flight paths of the neutrons to the detector were the same in each case. In this way, we were able to reduce systematic effects in the experiment to allow a direct comparison of the neutron survival fractions in the long and short slots for the same incident- and exit-beam conditions. Data were taken for both the long and short slots over a range of Bragg angles to confirm that the measurement technique yielded self-consistent results and to determine the backgrounds in the experiment.

### B. Crystal preparation

The slotted crystal was made by the Optics Fabrication and Metrology Group at the Argonne Laboratory Advanced Photon Source. A diamond impregnated saw blade cut each slot in a single operation to produce a uniform slot width of 1.9 mm. A standard milling machine was used to reduce the wall height by 12.7 mm over the downstream 37.5 mm of the slots. The crystal was cleaned to remove oil residue, but before etching the crystal to remove any damaged layers on the machined surfaces, we performed a reflectivity measurement to compare with that after etching. These results are discussed later in this paper.

Following this first set of measurements, the crystal was etched in a bath of hydrofluoric acid (4.8%), nitric acid (63.0%), and water (32.2%) for about 30 minutes. The crystal was slowly agitated in the bath and during the reaction, the bath temperature rose from 25 to 75 °C. The rate of material removal was approximately 200 $\mu$m over the 30 minutes such that the slot widths were enlarged to about 2.1 mm and the wall thickness reduced to about 1.7 mm. After cleaning, the etched crystal had a polished glasslike appearance as seen in Fig. 1.

## III. THE BRAGG SCATTERING PROCESS IN A PERFECT SILICON CRYSTAL

### A. Wavelength acceptance for Bragg scattering

The details of the Bragg scattering process in a perfect crystal have been developed for x rays using the dynamical theory [10–12] of crystal scattering. The extension of the theory to include neutrons has been reported elsewhere [13–16], and in this section, we only summarize the results needed to calculate the expected phase-space acceptance for Bragg scattering and the expected average reflectivity (the notation in this paper uses $k \equiv 2\pi/\lambda$, while many of the papers in the references use $k \equiv 1/\lambda$).

The condition that must be satisfied for a monochromatic beam of neutrons with a wavelength $\lambda_B$ to undergo Bragg scattering is given by [14]

$$2d \sin \theta_B = \lambda_B , \tag{1}$$

where $d$ is the interstitial spacing between the scattering planes, and $\theta_B$ is the scattering angle. For back scattering off the (440) planes in Si, the condition is satisfied for a wavelength $\lambda_B = 2d = 1.92$ Å. For a typical reactor beam with a broad range of wavelengths and angles, there will be a spread of Bragg angles and wavelengths satisfying Eq. (1).

When the Bragg condition is satisfied, some of the incident intensity will undergo a scatter off a particular set of planes as depicted in the lower diagram in Fig. 3. Some of the reflected intensity will escape the crystal, however, some will suffer a second reflection back into the crystal in the direction of the original beam and undergo further Bragg reflections inside the crystal. The dynamical theory of Bragg scattering takes these multiple-scattering effects [11] into account. In the quantum-mechanical description of the process [12,14], this results in the incident neutron flux splitting into two waves inside the crystal propagating parallel to the crystal surface. One wave has its maxima centered on the scattering centers, while the maxima of the second wave is between the scattering centers such that the two waves experience a different index of refraction and have slightly different velocities. Their combination gives rise to a wave with a ''beat'' pattern having a characteristic wavelength $\Delta_P$ that produces a back-and-forth energy flow in the crystal called ''Pendellösung.'' As the neutron wave propagates along the crystal slot, half the time the flow is into the crystal in the direction of the incident neutron, and half the time the flow is out of the crystal in the direction of the Bragg scattered beam. In general, if the crystal thickness is less than $\Delta_P$, there will be a transmitted as well as a reflected beam. If the thickness is much larger than $\Delta_P$, only the reflected wave exists.

The top plot in Fig. 3 shows the calculated intensity pattern for both a reflected and a transmitted beam for a nearly monochromatic parallel beam of neutrons incident on a 200 $\mu$m thick crystal. This calculation is performed in the plane-wave approximation [15] and the intensity is plotted against a normalized parameter [10] given by

$$y = -2\pi \Delta_e \Delta\theta \cos(\theta_B)/\lambda_B , \tag{2}$$

where $\Delta\theta$ is the deviation from the Bragg angle. The wavefunction extinction depth $\Delta_e$, where its amplitude is reduced by $e^{-1}$, is given by [13,14]

$$\begin{aligned} \Delta_e &= \sin(\theta_B)/[\lambda_B N_t b_c e^w] \\ &= [2dN_t b_c e^w]^{-1} \\ &= 0.0028 \ \text{cm}. \end{aligned} \tag{3}$$

The numerical result quoted in Eq. (3) is for the (440) planes in Si, where we used the neutron nuclear scattering length of

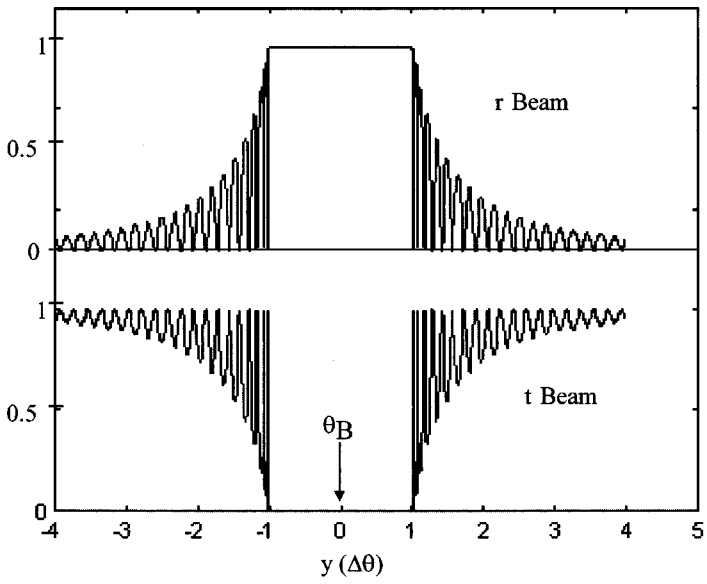


FIG. 3. An idealized "rocking" curve for a thin perfect Si crystal is shown plotted as a function of the normalized parameter $y=-2\pi\Delta_e\Delta\theta\cos\theta_B/\lambda_B$ taken from Ref. [10]. Thicker crystals do not have the transmitted beam.

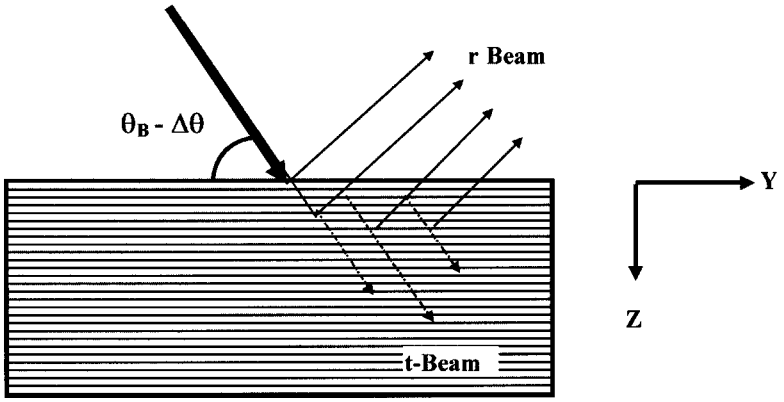


$b_c=0.42\times10^{-12}$ cm, the density of scattering centers of $N_t=0.50\times10^{23}$ atoms/cm$^3$, and the Debye-Waller factor [17] of $e^{-W}=0.885$ for scatters at room temperature.

For multiple reflections of neutrons down a slot cut into a perfect crystal each neutron retains its value of "$y$" over each successive scatter because the neutron energy is not altered during the Bragg scattering process. The fringes observed in the intensity plot in Fig. 3 at values of $|y|>1$ result from the Pendellösung energy flow. When the reflected intensity is calculated over many successive reflections, these fringes do not survive. However, the reflected intensity is unity for the range $|y|\leqslant1$. This highly reflective region is called the "Darwin peak." Neutrons that scatter within this peak remain there on each successive reflection such that they survive to the end of the slot even after thousands of reflections.

Analysis of the neutron energy flow across the Darwin peak shows that the wave function is maximized on the scattering centers at the edges and this gives rise to a neutron penetration depth into a perfect crystal that is deeper on average than that given by the extinction depth. The resulting neutron penetration into the crystal is given by [12,14]

$$L_p(y)=\Delta_e(1-y^2)^{-1/2}. \tag{4}$$

At $y=0$, $L_P=\Delta_e$, but increases dramatically as $|y|\to1$, giving rise to anomalous absorption at the edges of the Darwin peak. The average penetration over the entire Darwin peak yields

$$\begin{aligned}\Delta_p&=\int_{-1}^{+1}\Delta_e(1-y^2)^{-1/2}dy\\&=\pi\Delta_e\\&=0.0088\ \text{cm}.\end{aligned} \tag{5}$$

The $\Delta_P$ calculated in Eq. (5) is the same as the characteristic wavelength for the Pendellösung energy flow inside the crystal that was discussed above.

The angular width of the Darwin peak is found by combining Eqs. (2), (3), and (5) to yield

$$\begin{aligned}\Delta\theta_D(|y|\leqslant1)&=\lambda_B[2\pi\Delta_e\cos\theta_B]^{-1}\\&=2d[2\Delta_p]^{-1}\tan\theta_B\\&=1.1\times10^{-6}\tan\theta_B.\end{aligned} \tag{6}$$

The angular width of the Darwin peak varies from 6.2 $\mu$rad for $\theta_B=80°$ to 63.0 $\mu$rad for $\theta_B=89°$ for the (440) planes of

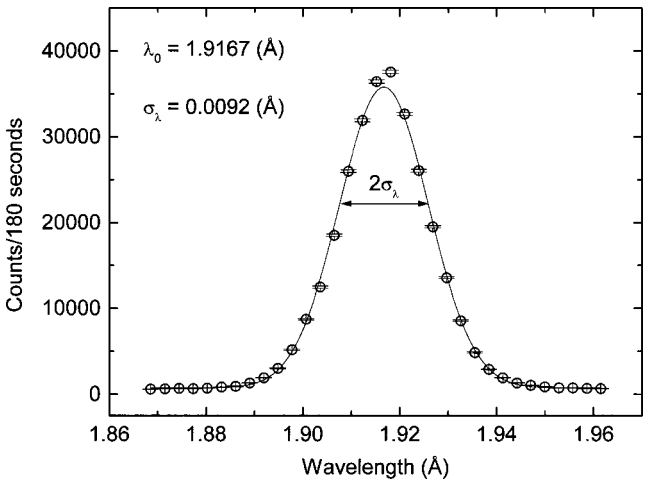


FIG. 4. The resulting neutron wavelength distribution following the double-crystal monochromator is shown after a measurement using reflections from the (220) planes in a small perfect Si crystal. The solid curve is a Gaussian fit to the data with the parameters shown.

Si. Within these angular widths there will be a spread in neutron wavelengths $\Delta\lambda_D$ (or equivalently, $\Delta k_D$) around the wavelength $\lambda_B$ that can be Bragg scattered for a given ray direction. This wavelength spread can be determined by taking the logarithmic derivative of Eq. (1),

$$\Delta\lambda_D/\lambda_B = \Delta k_D/k_B = \Delta\theta_D/\tan\theta_B = 1.1\times 10^{-6}. \tag{7}$$

Therefore, the reflected wavelength spread within the Darwin peak is independent of the Bragg angle.

### B. Phase-space acceptance for Bragg scattering in the crystal slots

The double-crystal monochromator produces a neutron beam characterized by a rms wavelength spread $\sigma_\lambda$ around a wavelength $\lambda_0$ within a horizontal angular divergence $\Delta\Theta_H$ and a vertical divergence $\Delta\Theta_V$. Therefore, the beam wavelength distribution $f(\lambda)$ has a Gaussian shape [9], such that the probability of finding the wavelength $\lambda_B$ within a narrow wavelength interval $\delta\lambda$ is given by

$$\delta f(\lambda_B) = [(2\pi)^{1/2}\sigma_\lambda]^{-1}\exp\{-(\lambda_0-\lambda_B)^2/(2\sigma_\lambda{}^2)\}\ \ \delta\lambda. \tag{8}$$

In our experiment, the double-crystal monochromator parameters were set to produce a beam with a central wavelength near 1.92 Å. The resulting wavelength distribution $f(\lambda)$ used in Eq. (8) was measured by placing a perfect Si crystal into the incident beam at the point where the slotted crystal would be mounted and measuring the rocking curve for reflections off the (220) planes. The results are shown in Fig. 4. The distribution had the expected Gaussian shape centered at $\lambda_0 = 1.9167$ Å and a rms width of $\sigma_\lambda = 0.0092$ Å indicating that the incident beam had a 1% wavelength spread (FWHM). It should be noted that at the slotted crystal, these beam parameters were independent of the Bragg angle $\theta_B$ that was chosen by rotating the crystal in the beam to reflect neutrons down the slots at a corresponding wavelength $\lambda_B$.

The incident wavelength rms spread $\sigma_\lambda/\lambda_0$ is much broader than the Darwin peak $\Delta\lambda_D/\lambda_B$ given by Eq. (7) for any particular value of $\lambda_B$. Therefore, other neutrons within the horizontal angular divergence $\Delta\Theta_H$ will Bragg reflect if they have wavelengths within the incident wavelength spread that satisfy Eq. (1). The total horizontal acceptance must take all of these neutrons into account.

The horizontal phase space acceptance ($A_H$) of the crystal slots will be the sum of the horizontal acceptances of each Darwin peak, $A_D = [\Delta\lambda_D/\lambda_B]\Delta\theta_D$, within the incident horizontal angular divergence and wavelength distribution $f(\lambda)$. The total acceptance may be estimated by multiplying $A_D$ by the ratio $[\Delta\Theta_H/\Delta\theta_D]$. However, $\Delta\theta_D$ is a function of the angle of the incident beam relative to the crystal slots, $\theta_B + \theta$, and therefore must be integrated over the incident distribution of neutron wavelengths given by Eq. (8). The resulting wavelength integral can be transformed to one over the angle $\theta$ using the differential form of Eq. (1): $d\lambda = 2d\cos(\theta_B+\theta)d\theta$. Taking the average value of the wavelength distribution over the angular width $\Delta\Theta_H$ to be $\langle f(\lambda_B)\rangle$, using Eqs. (6)–(7), and including the above factors, yields the horizontal acceptance

$$\begin{aligned} A_H(\theta_B) &= \{[\Delta\lambda_D/\lambda_B]\Delta\Theta_H\}\langle f(\lambda_B)\rangle \\ &\quad\times\int_{-\Delta\Theta_H/2}^{+\Delta\Theta_H/2}[1.1\times 10^{-6}\tan(\theta_B+\theta)]^{-1}2d \\ &\quad\times\cos(\theta_B+\theta)d\theta \\ &\cong[2d\cos^2\theta_B\Delta\Theta_H{}^2/(2.51\sigma_\lambda)] \\ &\quad\times\exp\{-(\lambda_0-\lambda_B)^2/(2\sigma_\lambda{}^2)\}. \end{aligned} \tag{9}$$

Because the Bragg angles in the experiment are close to 90° we have approximated the $\tan(\theta_B+\theta)$ by $1/\cos(\theta_B+\theta)$ to perform the integral in Eq. (9). As an example, we use the horizontal beam divergence of $\Delta\Theta_H = 11$ mrad and the wavelength rms spread of $\sigma_\lambda = 0.0092$ Å around a central value of $\lambda_0 = 1.9167$ Å, and calculate that the horizontal acceptance at a Bragg angle of 86° is $A_H = 4.8\times 10^{-5}$.

The horizontal phase-space acceptance calculated in Eq. (9) is for the first Bragg reflection in the slot. As mentioned above, the neutrons do not change their $y$ value upon reflection because the neutron energy is not changed during Bragg scattering. Therefore, we assume that once a neutron is within the horizontal acceptance it will continue to Bragg reflect down the slot unless it exceeds the vertical acceptance or is absorbed.

Finally, the above calculation assumes a plane-wave approximation. In reality, the neutrons have a spherical wave front when they strike the crystal and it may be questioned if this has an affect on the acceptance, particularly over thousands of reflections down the slot. A full spherical wave calculation may be performed using the methods developed in Ref. [16] for neutron interferometers where it is found that

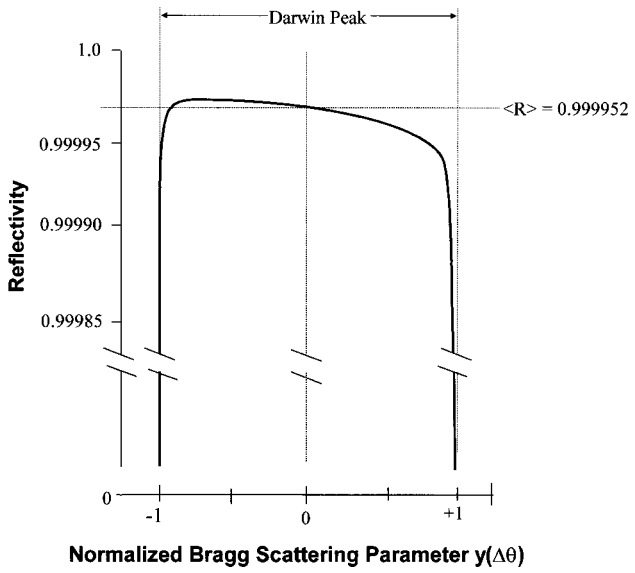


FIG. 5. The calculated reflectivity within the Darwin peak is shown for 1.92-Å neutrons after making multiple Bragg scatters off the (440) planes of Si. The reflectivity is less than unity due to absorption and diffuse thermal scattering in the crystal.

the plane-wave approximation yields acceptances and contrasts that are within 10% of the spherical results. However, the interferometer case is particularly sensitive to spherical wave fronts as coherence must be maintained over beams spatially separated by many centimeters. For 2.1-mm-wide crystal slots, the width of the beam entering any slot will be no more than 0.2 mm wide for the angles in our reflectivity experiment. The neutrons originate within the reactor at a distance of about 7 m and so the sagitta of the spherical wave front reflected down the slot will be less than the $d$ spacing of the crystal. Therefore, the plane-wave approximation provides sufficient accuracy for the acceptance calculation.

### C. Calculated reflectivity

The neutrons within the Darwin peak will suffer losses due to absorption ($\sigma_{\rm abs}$) and diffuse scattering ($\sigma_{\rm therm}$) within the crystal walls. This gives rise to a neutron reflectivity on each Bragg scatter that is slightly less than unity. This reflectivity can be calculated using the Prins-Darwin theory [10,11,15] where the crystal index of refraction is given an imaginary term to account for the losses. The resulting reflectivity curve for neutrons scattering within the Darwin peak off the (440) planes in Si is plotted in Fig. 5 as a function of the normalized $y$ parameter defined by Eq. (2).

The reflectivity varies across the Darwin peak due to differences in penetration depth given by Eq. (4). There is also a Pendellösung oscillation of the neutron wave function across the Darwin peak [12] that affects the absorption as one of the two split waves is centered on the atomic nuclei, while the other is not. Therefore, we expect a large absorption at the edges of the Darwin peak and significantly more absorption on one side of the Darwin peak than on the other. This is evident in the curve in Fig. 5 where the reflectivity decreases sharply at values of $|y|>0.9$. Neutrons within this range are expected to be lost after many successive reflections, and we have taken this loss into account by introducing an efficiency factor $\varepsilon_y=0.9$ in the calculated survival fraction.

After taking into account the losses at the edge of the Darwin peak, the average reflectivity $\langle R\rangle$ is found to occur at the center of the peak ($y=0$). From Eq. (4), the neutron penetration depth at this point is equal to $\Delta_e$ and the reflectivity is given by

$$\langle R\rangle=[1-\Delta_e N_t(\sigma_{\rm abs}+\sigma_{\rm therm})]. \tag{10}$$

Therefore, the survival fraction for $n_B$ successive Bragg reflections is given by

$$\eta=\varepsilon_y \exp[-n_B(1-\langle R\rangle)]. \tag{11}$$

As an example, the neutron trapping experiment of Schuster, Carlile, and Rauch [7] was performed using scatters off the (111) planes of Si that had an extinction depth $\Delta_e=0.000\,77$ cm. The cross section for absorption was $\sigma_{\rm abs}=0.596$ b, and the cross section for diffuse thermal scattering was $\sigma_{\rm therm}=0.161$ b at 293 K [18], yielding an expected reflectivity of $\langle R\rangle=0.999\,972$. This predicted that $\eta=\varepsilon_y e^{-1}=0.33$ n would survive over 35 000 reflections. Their experiment achieved over 2500 scatters, but due to losses occurring off the neutron guide tube surrounding the meter-long flight path between the Bragg reflecting walls they were only able to obtain a lower limit of $\langle R\rangle>0.9978$.

For our reflectivity experiment, the (440) planes of Si are used and the neutron velocity is higher, 2064 m/s, rather than 630 m/s for the experiment in Ref. [7]. The absorption cross section scales inversely with the velocity yielding $\sigma_{\rm abs}=0.182$ b. However, the cross section for diffuse thermal scattering is expected to be independent of velocity [18]. Using $\Delta_e=0.0028$ cm calculated using Eq. (3), yields a reflectivity from Eq. (10) of

$$\langle R\rangle=0.999\,952. \tag{12}$$

The survival fraction for $n_B$ successive Bragg reflections given by Eq. (11) is

$$\eta=\varepsilon_y \exp[-4.8\times10^{-5} n_B]. \tag{13}$$

This predicts that $\eta=\varepsilon_y e^{-1}=0.33$ of the neutrons will survive 21 000 successive Bragg reflections off the (440) planes of Si.

## IV. MEASURED RESULTS

### A. Geometric acceptances for the apparatus

During the reflectivity measurement, the vertical acceptance was set by the 10 mm high aperture placed in front of the detector. The 4 mm vertical dimension of the incident beam was set by the upstream Cd aperture, however, it expanded due to the vertical divergence as the beam traversed the crystal slots. Losses could occur if the beam grew to be larger than the detector aperture and this depended on the number of reflections down the slot.

The total neutron flight path from the Cd aperture to the detector is given by $L_D\,(\mathrm{mm}) = 136 + 48.9/\cos\theta_B$, where we used the average length of the long slots (48.9 mm). As described earlier, neutrons exiting the short slots are confined by the two end slabs resulting in the same total flight path $L_D$ as for the long slots. Therefore, the fraction of the vertical divergence $\Delta\Theta_V$ of the incident beam that will be observed in the detector is the same for the long and short slots and is given by

$$A_V = \mathrm{Min}\{1; 10/[4 + L_D \Delta\Theta_V]\} = \mathrm{Min}\{1; 10/[4.82 + 0.293/\cos\theta_B]\}. \quad (14)$$

This indicates that there would not have been any vertical loss in counts unless the Bragg angle exceeded 86.8°.

A similar loss of neutrons could occur due to the horizontal divergence if the beam grew beyond the 20 mm wide detector aperture. However, even for the neutrons reflecting in the 2.1 mm wide long slots, each slot acted like a funnel, such that the final beam reflected toward the detector had the same width as the beam that entered the slots. Therefore, the only horizontal expansion in the beam occurred after exiting the slots and this was minimal.

The last geometric acceptances concern the area $A_S$ of the incident beam accepted by the crystal slots and the probability $A_{\mathrm{EX}}$ that the neutrons exiting the slots will be directed toward the detector. At most, $A_S$ can equal the area of the incident beam ($0.4 \times 0.4 = 0.16\,\mathrm{cm}^2$). However, at the smallest crystal rotation angles the slots will not fill the available width of the incident beam. Furthermore, about half of the incident beam will strike the ends of the intervening slot walls and are presumably lost. In the experiment, we mounted the crystal relative to the pivot point of rotation for the table such that the first double-width slot would not be in the beam. Therefore, the parts of the crystal that can subtend the beam are the 17 narrow slots, the last double-width slot, and the 18 intervening walls. Using the average slot width of 2.1 mm, the average double-wide slot width of 4.1 mm, and the average wall thickness of 1.7 mm, the maximum beam area subtended by the slots is $A_S = 0.088\,\mathrm{cm}^2$ and occurs at a Bragg angle of 87°. Calculating the acceptance at other Bragg angles yields

$$A_S(\mathrm{cm}^2) = 0.088[\cos\theta_B/\cos(87°)] \quad (\text{for } \theta_B > 87°) = 0.086 \quad (\text{for } \theta_B \leqslant 87°). \quad (15)$$

The area of the beam exiting the slots will be the same as that entering the slots, however, neutrons will be directed toward the detector if the last reflection occurred off the slot wall farthest from the detector. If the last reflection took place on the opposing slot wall, the neutrons would be directed away from the detector and be lost. Due to the horizontal beam divergence $\Delta\Theta_H = 11$ mrad, there was a dispersion ($\delta n_B/n_B \approx \pm 6\%$) in the number of reflections down the slots. This implies that the last reflections were randomly distributed near the exit of the slots and that the probability that a neutron would be directed toward the detector was $A_{\mathrm{EX}} \sim 0.5$. However, the 2° bevel cut along the exit face of the crystal mentioned in Sec. II A acted to recover some of the misdirected neutrons. In fact, for Bragg angles larger than 88°, all neutrons would have been directed toward the detector. Therefore, the probability of detecting the neutrons upon exiting the slots is approximated by

$$A_{\mathrm{EX}} \cong 0.5[1 + \tan(2°)/\tan(90° - \theta_B)] \quad (\text{for } \theta_B < 88°) = 1.0 \quad (\text{for } \theta_B \geqslant 88°). \quad (16)$$

For example, at $\theta_B = 86°$ we calculate $A_{\mathrm{EX}} = 0.75$.

Combining the geometric acceptances with the horizontal phase-space acceptance and reflectivity calculated in the previous section permits the expected count rates to be computed as a function of the Bragg angle. The factors are

$$N(\theta_B) = \Phi A_S A_H A_V A_{\mathrm{EX}} \eta \varepsilon_D. \quad (17)$$

$\Phi$ is the incident flux, $A_S$ is the beam area subtended by the crystal slots, $A_H$ is the horizontal phase space acceptance, $A_V$ is the vertical acceptance, $A_{\mathrm{EX}}$ is the probability that the exiting neutrons are directed toward the detector, $\varepsilon_D$ is the detector efficiency (99% from Ref. [9]), and $\eta$ is the survival fraction after $n_B$ reflections due to an average reflectivity $\langle R \rangle$.

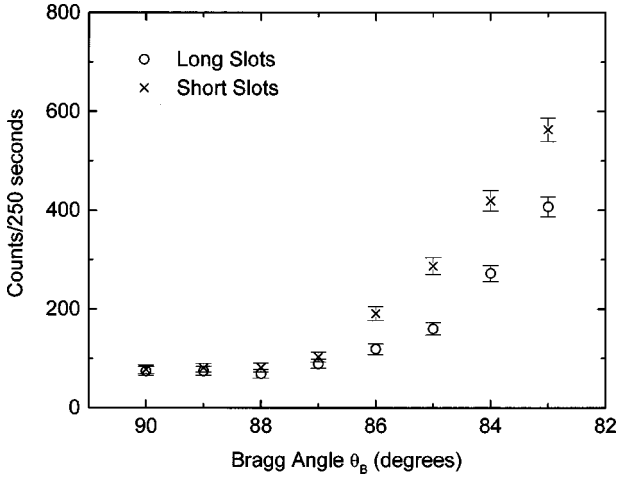


FIG. 6. The reflectivity data for the long and short slots are shown before the crystal was etched. They are plotted as the crystal was rotated in the incident beam. The errors are due to statistics. There is a significant difference observed between the long and short slots yielding a measured reflectivity of $\langle R \rangle = 0.9964$.

### B. Data

The observed count rates for both the long and short slots are plotted in Figs. 6 and 7 where the crystal has been rotated over a range of Bragg angles in the incident beam. The data in Fig. 6 are the results for the crystal before etching and the data in Fig. 7 are after etching. The error bars are due to statistics only.

The data in Fig. 7 is divided between (a) a rocking curve taken at successive rotation angles and (b) three high-statistics data points taken at specific angles. The technique for measuring each data set also differed. For the rocking curve, the crystal was rotated through all angles for the long

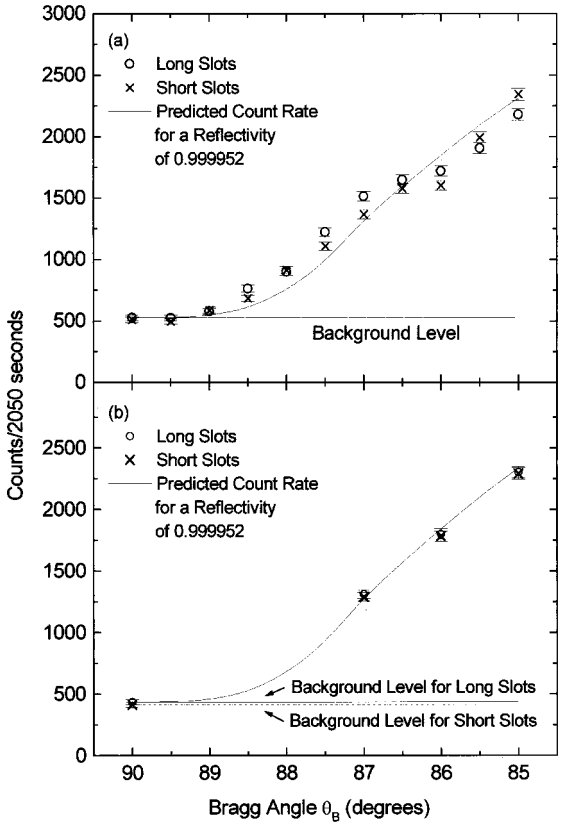


FIG. 7. The reflectivity data for the long and short slots are shown after the crystal was etched. The top figure (a) shows the rocking curve data. They are plotted as the crystal was rotated in the incident beam. The errors are due to statistics. The solid curve is the predicted count rates from Eq. (17) using the calculated acceptances in the experiment. There are no free parameters in this calculation. The bottom figure (b) shows the high-statistics data points used to measure the reflectivity. Unlike the data shown in Fig. 6 taken before etching the crystal, there is no significant difference observed between the long and short slots after subtracting backgrounds yielding a lower limit on the reflectivity of $\langle R\rangle > 0.9999$ at the 90% confidence level (see Table I).

slots and then rotated a second time for the short slots. The high-statistics data were taken by setting the crystal at a specific angle and counting for the long slots, and then lowering the crystal and counting for the short slots before moving to the next angle. This later method removed systematic effects due to angle nonreproducibility in the apparatus. The neutron background is also plotted in Fig. 7. It was determined from the asymptotic count rate at small rotation angles.

The solid curves in Fig. 7 are the predicted count rate at each angle calculated using Eq. (17). There are no free parameters in the calculation, however, if we allow the value of the incident flux to vary resulting in an overall normalization factor, the best curves yield a flux near $2.5 \times 10^5$ neutrons/cm$^2$/s that is in agreement with the expected flux. The agreement between the curves and the data, particularly for the high-statistics data points, demonstrates our understanding of the acceptances of the apparatus.

The general features of the data can be explained by the experimental parameters, for instance, the large wavelength spread in the incident beam allows Bragg reflections to occur over a broad range of angles. The approximately linear rise in counts at rotation angles up to 5° ($\theta_B = 85°$) follows the $\cos^2\theta_B$ dependence of the horizontal phase space acceptance given by Eq. (9).

The effect of a reduced reflectivity on the data would be a substantially reduced count rate for the long slots relative to the short slots at the same Bragg angle. Furthermore, the count rates for both the long and short slots would be expected to show a significant departure from the $\cos^2\theta_B$ dependence at small angles. Both of these effects are seen in Fig. 6 before the crystal was etched, whereas the data for the etched crystal in Fig. 7 is consistent with a large reflectivity. This clearly demonstrates the sensitivity of our technique to measure the reflectivity.

### C. Reflectivity measurement

To determine the reflectivity, we concentrated our high-statistics data comparison of count rates in the long and short slots at Bragg angles of 85.25°, 86.10°, and 87.15°. These angles were measured independently using a mechanical protractor and resulted in the noninteger values. The measured data are plotted in Fig. 7(b) and are also given in Table I after normalizing by the total counts on the beam monitor to yield counts per second of running time. The predicted count rates calculated from Eq. (17) agree with these data points.

When the ratio of the predicted count rates in the long versus short slots is formed, most of the factors in Eq. (17) cancel leaving only the exponential factor in $\eta$ from Eq. (11) that depends on the number of reflections and the average

TABLE I. The measured count rates ($N$) and the estimated backgrounds ($N_{\mathrm{BGD}}$) are quoted as neutrons/sec as a function of the Bragg angle $\theta_B$. The errors are due to statistics only. The average number of reflections down the slots is $\langle n_B\rangle$. The subscript $L$ refers to long slots, and $S$ refers to short slots. $R$ is the reflectivity calculated using Eq. (18). $N_{\mathrm{BDGL}} = 0.212 \pm 0.002$ n/s; $N_{\mathrm{BGDS}} = 0.201 \pm 0.002$ n/s. The average measured reflectivity is $\langle R\rangle = 0.999\,976$, yielding $\langle n_B\rangle = 42\,000$. However, the average measured reflectivity error is $\langle \delta R\rangle = \pm 0.000\,075$, yielding: $R(90\%\ \text{c. 1.}) > 0.9999$; and $n_B(90\%\ \text{c.1.}) > 10\,000$ (where $e^{-1}$ neutrons survive). Absorption and thermal scattering cross sections for reflections off the (440) planes in Si predict using Eq. (10): $R = 0.999\,952$; $n_B = 21\,000$.

| $\langle\theta_B\rangle$ | $N_L - N_{\mathrm{BGDL}}$ | $\langle n_{BL}\rangle$ | $N_S - N_{\mathrm{BGDS}}$ | $\langle n_{BS}\rangle$ | $R$ | $\delta R$ |
|---|---|---|---|---|---|---|
| 87.15° | $0.416 \pm 0.007$ | 466 | $0.420 \pm 0.007$ | 116 | 0.999973 | $\pm 0.000070$ |
| 86.10° | $0.652 \pm 0.008$ | 340 | $0.656 \pm 0.008$ | 85 | 0.999976 | $\pm 0.000070$ |
| 85.25° | $0.896 \pm 0.010$ | 279 | $0.900 \pm 0.012$ | 70 | 0.999979 | $\pm 0.000085$ |

reflectivity. Using the ratio of counts, the average reflectivity for a given crystal angle can be calculated using

$$\langle R\rangle = 1-(n_{BL}-n_{BS})^{-1}\ln[(N_S-N_{\mathrm{BGDS}})/(N_L-N_{\mathrm{BGDL}})], \tag{18}$$

where $n_B$ is the average number of reflections, $N$ is the number of counts, $N_{\mathrm{BGD}}$ is the number of background counts, and the subscripts $L$ and $S$ refer to the long and short slots, respectively.

The reflectivity results are given in Table I. For each of the three Bragg angles considered, the count rates for the long and the short slots are almost identical after background subtractions indicating a large reflectivity. When the three values are averaged together, they yield a measured reflectivity of $\langle R\rangle = 0.999\,976$. However, from the propagation of the statistical errors through Eq. (18) we arrive at an average rms error on the reflectivity of $\langle \delta R\rangle = \pm 0.000\,075$. Therefore, the measured reflectivity is most likely larger than is warranted by the statistics. However, the rms error allows us to place a 90% c. 1. lower limit on the reflectivity and on the average number of reflections where $\varepsilon_y e^{-1}$ of the neutrons survive

$$\langle R\rangle > 0.9999,$$

$$\langle n_B\rangle > 10.000 \quad (90\%\ \text{c.l. lower limit for}\ \lambda \cong 1.92\ \text{Å}). \tag{19}$$

These results are considerably larger than the lower limits quoted in the last section for the experiment of Schuster, Carlile, and Rauch [7]. They may also be compared to the calculated values using Eq. (10) assuming only absorption and thermal scattering losses. For $\lambda = 1.92$ Å the calculated values are $\langle R\rangle = 0.999\,952$ and $\langle n_B\rangle = 21\,000$, such that the results in Eq. (19) are consistent with these predictions.

Finally, the background level evident in Fig. 7(b) differs slightly for the long and short slots. We believe these backgrounds are due to thermal scattering in the crystal walls. The background is smaller for the shorter slots, which is consistent with the thermal scattering hypothesis as less material is encountered by these neutrons. Furthermore, the backgrounds evident in Fig. 6 taken before the crystal was etched are 50% larger than that for the etched crystal and the measured reflectivity is substantially reduced to $\langle R\rangle = 0.9964$. A possible explanation for the reduced reflectivity is that the machining process left strains in the slot walls disrupting the homogeneity in the bulk crystalline structure allowing deeper neutron penetration. Such effects have been observed in neutron interferometers [19]. Etching the crystal in the solution of hydrofluoric and nitric acids successfully removed this strained layer, allowing the bulk crystal to relax to its original state resulting in a significant increase in the reflectivity.

## ACKNOWLEDGMENTS

The authors wish to thank the University of Missouri Research Reactor Staff. Also, we want to acknowledge the diligent help of Jared Bowden and Hunter Husar during the time that our measurements were taken. S.A.W. also wishes to acknowledge support from NSF Grant No. PHY 9603559.

[1] For instance, see N. Ramsey, Rep. Prog. Phys. **45**, 95 (1982), and references cited therein.
[2] K. F. Smith *et al.*, Phys. Lett. B **234**, 191 (1990).
[3] C. Shull and R. Nathans, Phys. Rev. Lett. **19**, 384 (1967).
[4] T. Dombeck, Proceedings of 8th Meeting of DPF, edited by S. Seidel, (Albuquerque 1994), Vol. 1, p. 948.
[5] T. Dombeck, Argonne National Laboratory Report No. PHY-8624-HI-97 (unpublished).
[6] T. Dombeck, H. Kaiser, D. Koetke, M. Peshkin, and R. Ringo, Argonne National Laboratory Report No. PHY-9814-TH-2001 (unpublished).
[7] M. Schuster, C. Carlile, and H. Rauch, Z. Phys. B: Condens. Matter **85**, 49 (1991).
[8] E. Jericha, C. Carlile, and H. Rauch, Nucl. Instrum. Methods Phys. Res. A **379**, 330 (1996).
[9] B. Allman *et al.* Nucl. Instrum. Methods Phys. Res. A **412**, 392 (1998).
[10] W. Zachariasen, *Theory of X-Ray Diffraction in Crystals* (Dover, New York, 1994).
[11] R. W. James, *The Optical Principles of the Diffraction of X-Rays* (Ox Bow Press, Woodbridge, CT, 1962).
[12] B. Batterman and H. Cole, Rev. Mod. Phys. **36**, 681 (1964).
[13] M. Goldberger and F. Seitz, Phys. Rev. **71**, 294 (1947).
[14] V. F. Sears, Can. J. Phys. **56**, 1261 (1978).
[15] U. Bonse and W. Graeff, Top. Appl. Phys. **22**, 93 (1977).
[16] W. Bauspiess, U. Bonse, and W. Graeff, J. Appl. Crystallogr. **9**, 68 (1976).
[17] C. Kittel, *Introduction to Solid State Physics* (Wiley, New York, 1966); U. Bonse, in *Neutron Interferometry*, edited by U. Bonse and H. Rauch (Clarendon, Oxford, 1979).
[18] K. Binder, Phys. Status Solidi **41**, 767 (1970).
[19] H. Rauch and S. A. Werner, *Neutron Interferometry* (Oxford Science Publications, Clarendon, Oxford, England, 2000), p. 31.